Geophys. J. Int. (1995) **123**, 232–244

Rock-magnetic proxies of climate change in the loess–palaeosol sequences of the western Loess Plateau of China

Christopher P. Hunt,[1] Subir K. Banerjee,[1] Jiamao Han,[2] Peter A. Solheid,[1] Eric Oches,[1] Weiwei Sun[1] and Tungsheng Liu[2]

[1]*Institute for Rock Magnetism, University of Minnesota, Minneapolis,* MN 55455, *USA*

[2]*Institute of Geology, Chinese Academy of Sciences, Beijing, China*

Accepted 1995 May 5. Received 1995 April 21; in original form 1994 November 8

SUMMARY

Results of the first detailed study of the climate proxy record in the loess–palaeosol sequence at Xining—one of the few palaeoclimate sites in the currently arid western Loess Plateau of China—illustrate the importance of making many types of rock-magnetic measurements other than susceptibility. A multiparameter approach yielded confirmation that here, as elsewhere in the Loess Plateau, the susceptibility enhancement in palaeosols was caused primarily by ultrafine magnetite and maghaemite. Nevertheless, magnetic enhancement was caused not exclusively by changes in relative grain size, but also by variations in concentration and mineralogy of the magnetic fraction.

The effects of concentration variations were removed through normalization of susceptibility and anhysteretic remanence with saturation magnetization and saturation remanence, respectively. The resulting signal was ascribed more confidently to variation in magnetic grain size, which in turn was interpreted as a better proxy of pedogenesis than simple susceptibility. Variations in magnetic mineralogy were also determined to constrain interpretations further. The data were then used to discuss climate history at Xining. Finally, results from Xining were compared with other western sites and contrasted with eastern sites.

In summary: (1) data is presented from a new Loess Plateau site which also appears to yield a global climate signal; (2) a demonstration is made of a more rock-magnetically robust way to separate concentration, composition and grain-size controls on susceptibility and other magnetic parameters; and (3) models are provided for inter-regional comparisons of palaeoclimate proxy records.

Key words: China, climate, loess, magnetism, mineralogy, palaeosol.

INTRODUCTION

Palaeoclimate studies

Sequences of loess and interbedded palaeosols blanket a 440 000 km^2 area in north-central China to depths of up to 300 m (Liu 1991) (Fig. 1). These sequences contain east-Asian palaeoclimate proxy information for much of the Quaternary. Low-field magnetic susceptibility time-series from numerous sites in the Loess Plateau correlate well with marine sediment $\delta^{18}O$ data (Heller & Liu 1984; Kukla 1987; Kukla *et al.* 1988; Hovan *et al.* 1989; Maher & Thompson 1992; Liu & Ding 1993; Banerjee 1995), which have been interpreted as a global ice-volume signal and hence as a proxy for global climate change (Imbrie *et al.* 1984; Heller & Liu 1986). Magnetic susceptibility tends to be higher in the palaeosols that formed during the relatively warmer and wetter interglacial periods. Thus, the magnetic susceptibility of loess–palaeosol sequences appears to be related to climatic conditions.

There has been much debate over the cause of the susceptibility enhancement, and numerous models have been proposed to explain the mechanism, including provenance shifts, changes in wind velocity, fires, and so on (for a summary, see Eyre & Shaw 1994). Two schools of thought, however, have received the most attention. The first group maintains that a uniform tropospheric magnetite rain is diluted to varying degrees by the weakly magnetic loess material blowing in from the source regions to the north-west of the Loess Plateau. Colder and drier periods bring more dust and hence dilute the rain more, leaving the susceptibility of the palaeosol layers relatively higher (Kukla *et al.* 1988). The second school suggests that the susceptibility enhancement is due to *in situ* pedogenesis, whereby new magnetic material forms in place as part of soil development during warmer and wetter times (Maher & Taylor

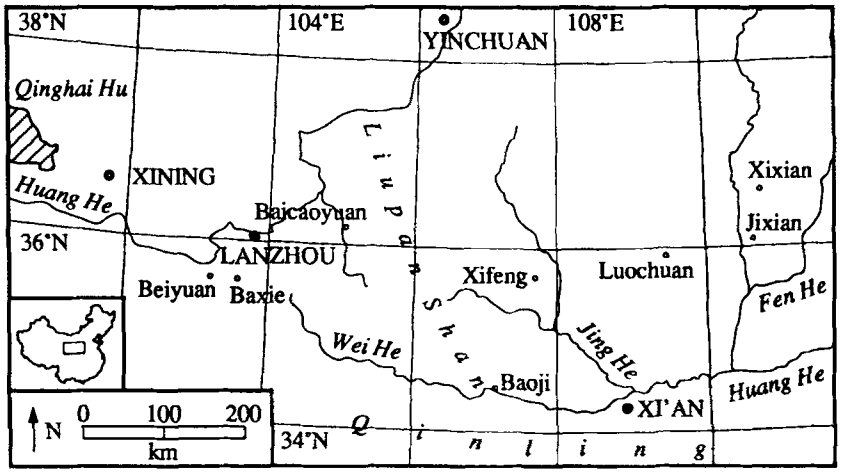

Figure 1. Map of the Loess Plateau of north-central China. The Liupan Shan range divides the plateau into a drier western part and a wetter eastern part. Xining is located at the western edge (36.6°N, 101.7°E).

1988; Zhou *et al.* 1990; Maher & Thompson 1991; Heller *et al.* 1993). Among the latter group, authors have ascribed pedogenic enhancement to decalcification and soil compaction (Heller & Liu 1984, 1986), to grain-size differences between loess and palaeosol (Zhou *et al.* 1990; Maher & Thompson 1991; Maher & Thompson 1992), or to mineralogy differences between loess and palaeosol (Han *et al.* 1991; Hus & Han 1992; Maher & Thompson 1992; Verosub *et al.* 1993; Evans & Heller 1994; Eyre & Shaw 1994).

Recent efforts have also attempted to unravel the links between magnetic variables and climate changes, both on global and on local or regional scales. Studies of low-temperature magnetic behaviour of loess and palaeosol samples have established a semi-quantitative relationship between the amount of ultrafine magnetite and the degree of soil development, which in turn was related to climatic conditions (Banerjee, Hunt & Liu 1993). This work was extended (Heller *et al.* 1993; Liu *et al.* 1995) to derive a quantitative magnetic palaeoprecipitation parameter for the region. Maher, Thompson & Zhou (1994) have also derived palaeoprecipitation values for a number of sites in the Loess Plateau based on the enhancement of susceptibility in the *B*-horizons of soils and palaeosols.

We provide here the first detailed study of the loess section at Xining and compare it with studies of other sites in the western Loess Plateau to arrive at an overall picture of the climate-change record in the region.

The Xining section

The Dadunling site, a few kilometres north of Xining (36.6°N, 101.7°E), is located at the drier western edge of the Loess Plateau (Fig. 1). Compared with sites farther east, Xining currently has a relatively cooler and drier climate, similar to other nearby sites such as Beiyuan (about 170 km south-east), Lanzhou (about 190 km east-south-east) and Baicaoyuan (about 300 km east). All of these sites lie to the west of the Liupan Mountains, which cause a (current) rain-shadow of the east-Asian monsoon. There is evidence, however, that the western sites were not always drier than the eastern sites (Maher *et al.* 1994), so the climate record from the west may yield insights into the history of the regional response to changing Asian monsoons, imprinted over the global signal. Because information from western sites is sparse, data from Xining are critical for an understanding of processes of atmospheric moisture transport in the past, and can therefore contribute to improved palaeoclimate models.

A previous pedologic and palaeostratigraphic study of the Xining section found it to have the thickest, most complete loess profile in Qinghai Province, being composed of the Holocene, Malan, Lishi, and part of the Wucheng loesses (Li, Ma & Zeng 1992). The total thickness of the profile is 267 m, and the maximum age at the base is approximately 1.2 Ma. A preliminary magnetic study (Oldfield, Chen & Wu 1994) found unimodal, relatively coarse ferrimagnets in the loess, and this coarse fraction plus a finer fraction was identified in the palaeosols. In this study, we were interested only in the record of the last two glacial cycles (corresponding to marine $\delta^{18}O$ stages 1–6, or approximately the last 130 ka), which produced the Holocene [L_0 and S_0 (following the designations of Kukla & An 1989)], Malan (L_1), and the very top of the Lishi (S_1 and top of L_2) layers. Li *et al.* (1992) very briefly describe this part of the Xining section as follows (paraphrasing).

The Holocene loess (L_0–S_0) has a thickness of 0.6 m. The upper sublayer (L_0) has a thickness of 0.1 m and consists of a dark grey sandy silt. The lower sublayer (S_0) has a thickness of 0.5 m and consists of a grey-black clayey silt. The Malan loess (L_1) has a thickness of 16.6 m and consists of porous and loose light yellow-grey sandy silt. Within L_1 there are two strong weathered yellow-brown thin clayey silt layers of thicknesses 0.6 and 0.3 m. In the Lishi loess (S_1-L_{15}, total thickness of 232.8 m), S_1 has a thickness of 7.1 m, and contains three palaeosol sublayers and two loess layers. The upper two weakly developed palaeosols (S_1SS_1 and S_1SS_2) are yellow-brown; the lower mature palaeosol (S_1SS_3) is dark brown to red-brown.

Finally, L_2 has a thickness of 12.6 m and consists of light yellow-grey sandy silt.

The above authors estimated dates and deposition rates based on an assumed linear deposition rate between known palaeomagnetic markers such as the Blake event (they use 114 ka), found at 21.0 m depth in the middle of S_1, and the Brunhés–Matuyama boundary (they use 730 ka) found at 146.8 m depth at the top of L_8. The average deposition rate for the layers of interest was thus approximately 0.18–0.20 mm a^{-1}

(Li *et al.* 1992). Use of the recently corrected date of 790 ka for the Brunhés–Matuyama boundary (Baksi *et al.* 1992) would not alter these rates significantly.

Sampling technique

Because the Malan loess is draped over the underlying layers on the hillside at Xining, our field work for this study began by digging a trench downslope to a depth of up to 3 m in order to ensure that the true section was sampled. Smooth vertical faces were carved into the easily worked loess. The lowest S_1 sublayer was identified visually based on information from Li's study, and located precisely with a field susceptibility coil. Sampling commenced about 1.25 m below this point in the upper part of L_2. Bag samples (approximately 150 g) were taken at 10 or 20 cm intervals up a smoothed fresh face, with horizontal displacements every few samples to move upslope in a stair-step fashion. Occasionally, field duplicates were obtained, especially at horizontal steps. A 20 m horizontal offset occurred approximately 7 m below the L_1/S_0 boundary (depth approximately 9.5 m below the top of the section), when sampling moved from the hillside trench to a hilltop pit. Approximately 30 m of the profile were sampled, from the upper part of L_2 to near the top of S_0. Because the uppermost layer L_0 lies within the current agricultural plough zone just below the surface, it is likely to be disturbed and was therefore not sampled. In the laboratory, subsamples from the bags were weighed (approximately 10 g) and packed into plastic boxes (approximately 6 cm^3) for magnetic analysis. The remainders were saved for other magnetic measurements and non-magnetic treatments.

RESULTS

Magnetic susceptibility and hysteresis measurements

In order to compare our results with previous studies from other sites, the magnetic low-field susceptibility, χ, was first measured for all samples with a Bartington susceptibility bridge. All samples were then given an anhysteretic remanent magnetization, σ_{arm}, in a peak alternating field of $\mu_0 H = 100$ mT and a steady field of $\mu_0 H = 50$ μT using a modified Schonstedt alternating-field demagnetizer. Remanences were measured on a 2G cryogenic magnetometer. Repeated measurements on the same sample showed that the experimental uncertainties in susceptibility and remanence were within 1 per cent. Uncorrected mass-specific susceptibility values varied in the range $\chi = 2.1\text{–}7.6 \times 10^{-7}$ m^3 kg^{-1}, with the lowest values in the loess layers, and the highest in the palaeosol layers (Fig. 2a). Mass-specific anhysteretic remanence values varied in the range

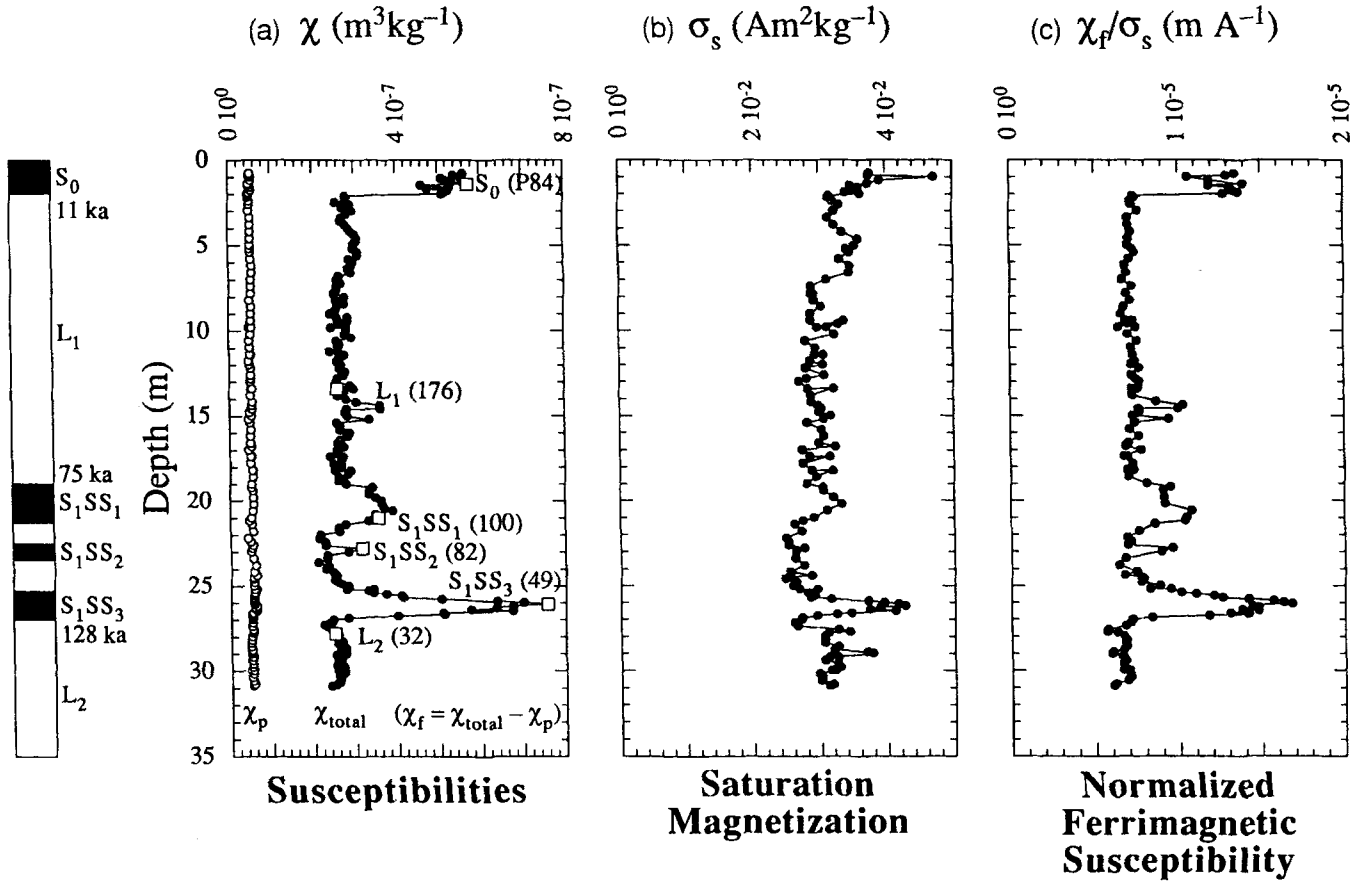

Figure 2. Loess/palaeosol stratigraphy at Xining, with approximate dates for the boundaries between layers. (a) Low-field total magnetic susceptibility, χ_{total}, for all samples, and paramagnetic susceptibility, χ_p, for approximately half of the samples. Labelled open squares denote samples which were selected to be representative of their layers and which were subjected to more detailed measurements. (b) Saturation magnetization, σ_s, for approximately half of the samples. (c) Normalized ferrimagnetic susceptibility, $(\chi_{total}-\chi_p)/\sigma_s$, which represents the concentration-independent variation of (mostly) SP magnetite.

$\sigma_{arm} = 0.2–2.1 \times 10^{-4}$ A m^2 kg^{-1}, again with the lowest values in the loess layers and the highest in the palaeosol layers (Fig. 3a).

The lithologic boundaries between the various loess and palaeosol layers were then finalized based on field colour and texture observations and on field and laboratory susceptibility values. Within S_1, three distinct palaeosol sublayers were identified and labelled from the uppermost to the lowest as S_1SS_1, S_1SS_2, and S_1SS_3. The ages of the boundaries were taken to be the accepted values of 128 ka for L_2/S_1, 75 ka for S_1/L_1, 11 ka for L_1/S_0, and 0 ka for the surface (after Heller & Liu 1984; Imbrie *et al.* 1984; Heller & Liu 1986; Kukla *et al.* 1988). These ages would change only marginally if the new recommendations for stage boundaries at low latitudes (Bassinot *et al.* 1994) were used.

In order to obtain intrinsic magnetic parameters, hysteresis loops were measured for every other sample with a Princeton Applied Research vibrating sample magnetometer. Experimental uncertainties in hysteresis parameters were estimated to be within about 2 per cent. Mass-specific saturation magnetization values varied in the range $\sigma_s = 2.4–4.7 \times 10^{-2}$ A m^2 kg^{-1}, with the lowest values in the loess layers and the highest in the palaeosol layers (Fig. 2b). Mass-specific saturation isothermal remanence values varied in the range $\sigma_{rs} = 2.9–7.1 \times 10^{-3}$ A m^2 kg^{-1}, again with the lowest values in the loess layers and the highest in the palaeosol layers (Fig. 3b).

The mass-specific paramagnetic susceptibility, χ_p, of the 'non-magnetic' minerals (mainly clays) in the samples was obtained from the high-field slope of the hysteresis curves. Values were nearly uniform throughout the section, with a value of about $\chi_p = 0.5 \times 10^{-7}$ m^3 kg^{-1} (Fig. 2a). The mass-specific, purely ferrimagnetic susceptibility, χ_f, was calculated as the difference between the raw bridge susceptibility and the paramagnetic susceptibility, i.e., $\chi_f = \chi - \chi_p$.

Both susceptibility and anhysteretic remanence are concentration-dependent parameters; they depend to the first order on the amount of magnetic material present. To remove the effects of concentration and thereby see only the intrinsic changes in the grain size or mineralogy of the magnetic carrier, the ferrimagnetic susceptibility and anhysteretic remanence were normalized respectively by room-temperature saturation magnetization, σ_s (a measure of the total size-independent magnetic content), and room-temperature saturation isothermal remanence, σ_{rs} (the maximum remanence achievable). Normalized ferrimagnetic susceptibility varied in the range $\chi_f/\sigma_s = 0.6–1.7 \times 10^{-5}$ m A^{-1}, and normalized anhysteretic remanence varied in the range $\sigma_{arm}/\sigma_{rs} = 0.6–3.0 \times 10^{-2}$, with the lowest values in the loess layers and the highest in the palaeosol layers (Figs 2c and 3c).

Other magnetic measurements

Further measurements were made on selected samples chosen to be representative of the various layers (S_0, L_1, S_1SS_1, S_1SS_2,

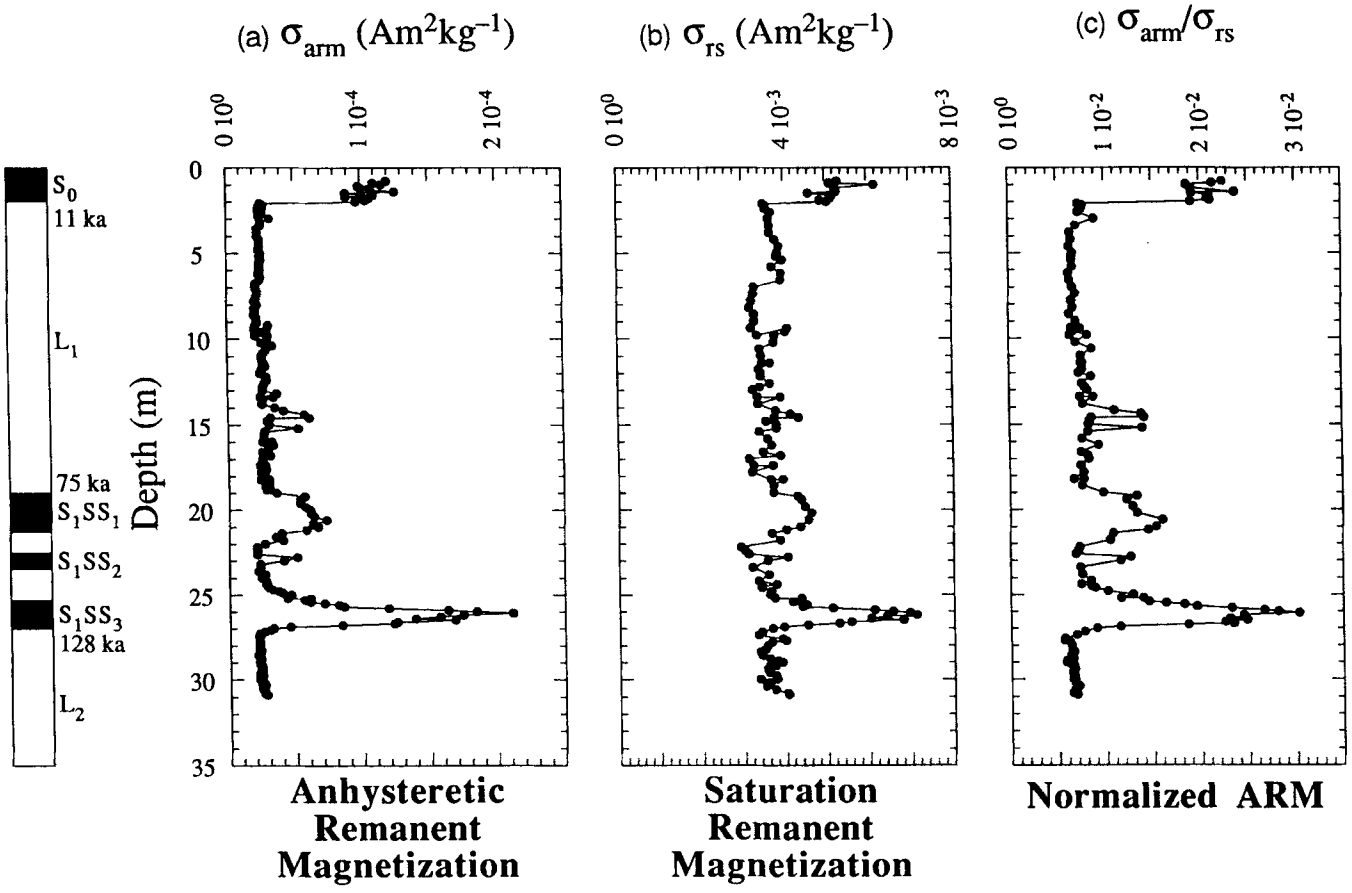

Figure 3. (a) Anhysteretic remanent magnetization, σ_{arm}, for all samples. (b) Saturation remanent magnetization, σ_{rs}, for approximately half of the samples. (c) Normalized anhysteretic remanence, σ_{arm}/σ_{rs}, which represents the concentration-independent variation of (mostly) SD and PSD magnetite.

S_1SS_3 and L_2), as determined from susceptibility values (see Fig. 2a).

Thermal demagnetization of a low-temperature (20 K) saturation isothermal remanent magnetization was performed with a Quantum Design susceptometer (Fig. 4). The relative amounts of ultrafine magnetic material can be estimated from the resulting curves: the change in remanence between 20 K and room temperature, not including the Verwey–transition step near 118 K, reflects the unblocking of those uniformly magnetized grains which are called 'superparamagnetic' (SP) at room-temperature (proposed by Néel 1949; coined by Bean & Livingston 1959; reviewed by Cullity 1972). The presence of the Verwey transition in the remanence data from all samples (Fig. 4) indicates that sufficiently large (d > SP) and chemically pure magnetite grains also exist (Özdemir, Dunlop & Moskowitz 1993). Graphical analysis of these curves according to the method of Hunt & Banerjee (1992) yields the proportion of 20 K saturation isothermal remanence that is carried by grains of magnetite and maghaemite that are SP at 300 K (Fig. 9). This technique assumes that the field during warming is sufficiently small that the induced magnetization is negligible. Using the largest measured susceptibility at any temperature ($\chi = 1 \times 10^{-6}$ m^3 kg^{-1}) and the largest measured 'zero' field ($\mu_0 H = 300$ μT, or $H = 240$ A m^{-1}), we calculate that the largest induced magnetization was $\sigma_{induced} = \chi H = 2.4 \times 10^{-4}$ A m^2 kg^{-1}, which is more than an order of magnitude smaller than the smallest remanence measured in this way. Thus, the contribution of the induced magnetization may be ignored.

The frequency dependence of susceptibility (at room temperature) between 10 Hz and 10 000 Hz was determined with a Lake Shore susceptometer (Fig. 5). The frequency dependence of susceptibility data also suggests that the most developed soils contain both absolutely and relatively more SP particles, because susceptibility decreases with increasing frequency for a distribution of such particles (Stephenson 1971; Bloemendal, Barton & Radhakrishnamurty 1985). Fig. 5 also demonstrates the problems associated with measuring the frequency dependence as a percentage change between two susceptibility values (known as the F-factor or χ_{fd}). Using the points labelled in the figure (those conventionally measured by a Bartington dual-frequency bridge), one would find values of 0.8 per cent for the L_2 loess and 7.8 per cent for the S_1SS_3 palaeosol. However, these values have large uncertainties because they are calculated from the differences between two large numbers whose experimental uncertainties are often of the same order as the differences. A more complete presentation of the data (as in Fig. 5) avoids this problem and simultaneously gives information about the grain-size distribution (Stephenson 1971).

The low-temperature dependence of susceptibility (at 730 Hz) between 15 K and room temperature was determined with a Lake Shore susceptometer. The high-temperature dependence of susceptibility (at 920 Hz) between room temperature and 973 K (700 °C) was measured with a furnace-equipped Kappabridge (Fig. 6). In the resulting curves, the plateau seen between approximately 120 K (−153 °C) and 600 K (327 °C) for the more developed palaeosol samples corresponds to a superparamagnetic–single-domain transition on cooling. The peak seen between approximately 120 K (−153 °C) and 220 K (−53 °C) for the loess and less developed palaeosol samples corresponds to multidomain material (Radhakrishnamurty & Deutsch 1974). Because the paramagnetic susceptibility of other minerals (iron-bearing silicates) in the sample varies inversely with absolute temperature, the signal increases sharply at the lowest temperatures when it is dominated by χ_p.

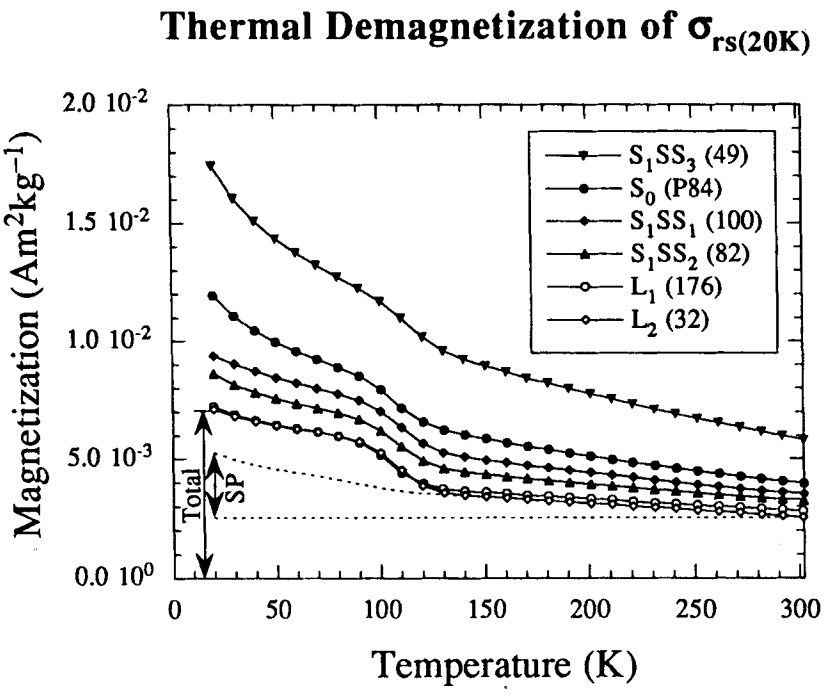

Figure 4. Low-temperature thermal demagnetization for selected samples of a saturation isothermal remanent magnetization, σ_{rs}, imparted at 20 K. The loss of remanence between 20 K and 300 K indicates the presence of SP particles. Note that the effect is greatest in the more developed soils, S_0 and S_1SS_3. The step near 118 K is caused by the Verwey transition in magnetite. Note that the magnitudes of the transitions are, in absolute terms, roughly equal in all samples, but relatively more important in loess layers.

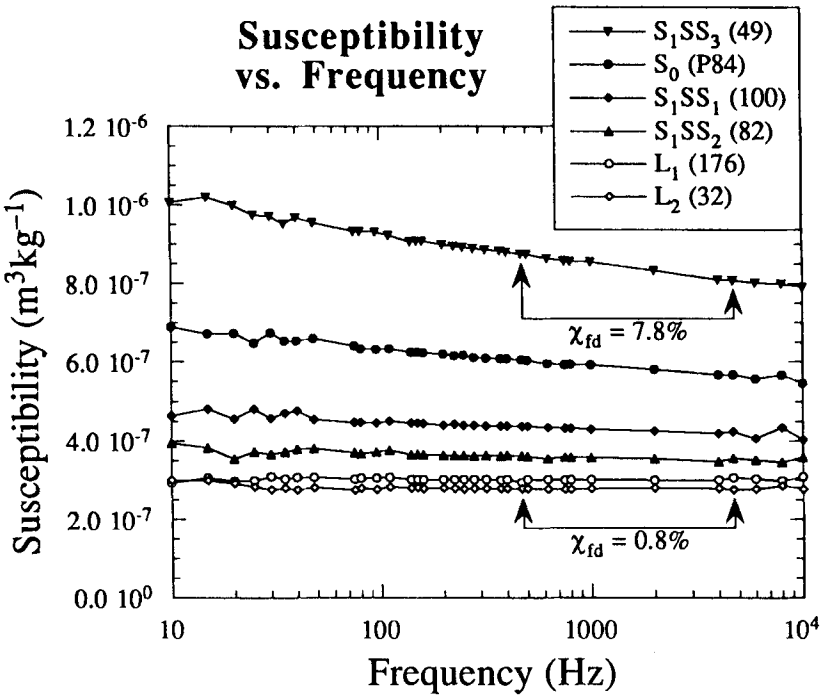

Figure 5. Frequency dependence of susceptibility for selected samples at room temperature. The loss of susceptibility with frequency indicates the presence of SP particles. Note that the effect is greater in the more developed soils, S_0 and S_1SS_3. (See text for an explanation of χ_{fd} values.)

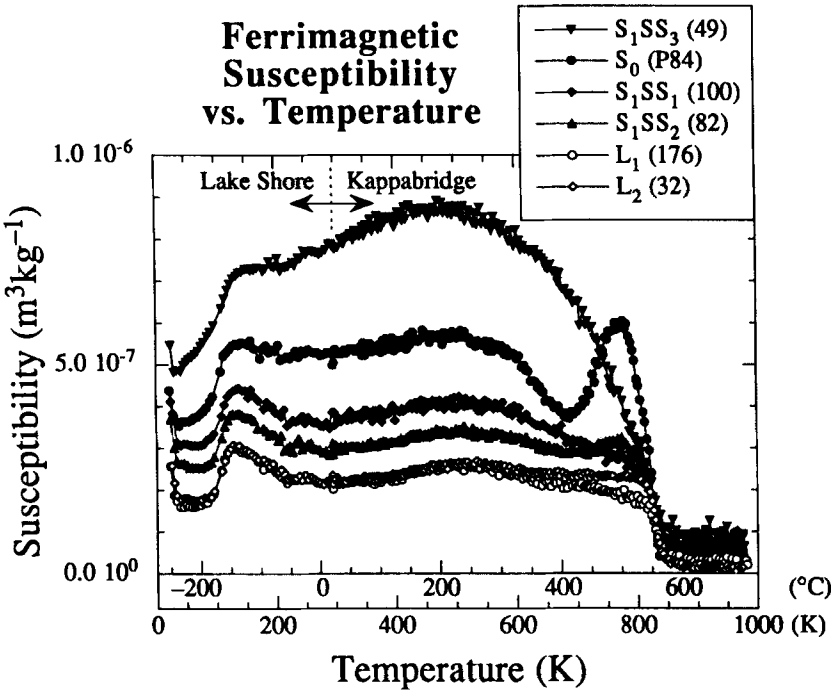

Figure 6. Temperature dependence of ferrimagnetic susceptibility for selected samples. Note the Verwey transition near 118 K and the uniform Curie temperature near 845 K (572 °C), both of which show that much of the susceptibility signal is carried by magnetite. Because the Kappabridge had not been calibrated with an appropriate susceptibility standard of the correct size and shape, the room-temperature Kappabridge values were about 20 per cent higher than the room-temperature Lake Shore values, which had been properly calibrated. The Kappabridge data were therefore corrected to match the Lake Shore data at room temperature. Also, the $1/T$ dependence of the paramagnetic susceptibility, χ_p, has been subtracted from the data.

Further evidence for magnetite comes from the temperature dependence of susceptibility curves, in which the Verwey transition appears again as a step near 118 K (−155 °C), and the Curie point is near 845 K (572 °C) for all samples (Fig. 6).

The higher organic carbon content in S_0 (see below) is responsible for the creation of magnetite from iron-bearing clay minerals or haematite upon heating under reducing conditions. (Although the Kappabridge sample-analysis tube

is open to the air and the top of the sample often turns red because of the oxidation of magnetite and maghaemite to haematite, the presence of other minerals and organic carbon create a locally reducing atmosphere for the bulk of the sample, which remains dark). All samples display magnetite cooling curves (not shown here), but the process is more pronounced in S_0.

Non-magnetic measurements

Mössbauer

Mössbauer absorption spectra for magnetic extracts from four samples [S_0, L_1, S_1SS_3 and L_2 (see Fig. 2a) were obtained with a Ranger spectrometer using a ^{57}Co source. Because the Mössbauer effect is sensitive to the valence states of ^{57}Fe atoms in a crystal lattice, and because the area of a spectrum is proportional to the number of ^{57}Fe atoms in a given valence state and coordination, it was possible to analyse the spectra to determine the proportion of maghaemite (γ-Fe_2O_3) in the ferrimagnetic fraction (maghaemite plus magnetite) (Fig. 7). The room-temperature spectrum for magnetite is resolved into two sextets, the first from octahedral Fe^{2+} and Fe^{3+} (sometimes denoted as $Fe^{2.5+}$), and the second from tetrahedral Fe^{3+}. Maghaemite, which has only Fe^{3+} in both the octahedral and tetrahedral sites, appears as one sextet which overlaps with the sextet from the tetrahedral site of magnetite.

For pure magnetite, which has an inverse spinel crystal structure, two-thirds of the Fe is in the octahedral site in the form of Fe^{2+} and Fe^{3+} ions. Electron hopping among the ions produces an averaged sextet characterized by a hypefine field of $B_{hf}=46.0$ T, a quadrupole splitting of $\Delta E_Q \approx 0$ mm s^{-1}, and an isomer shift of $\delta_{Fe}=0.66$ mm s^{-1} (fit no. 1 in Table 1). The tetrahedral site contains one-third of the Fe in the form of Fe^{3+} ions, which produce a sextet with $B_{hf}=49.1$ T and $\Delta E_Q \approx 0$ mm s^{-1} (included in fit no. 2 in Table 1). Maghaemite has only Fe^{3+} ions, which are distributed in octahedral and tetrahedral sites; it produces one sextet with $B_{hf}=50.0$ T (also included in fit no. 2 in Table 1) (Vandenberghe *et al.* 1990). As the proportion of maghaemite increases in a mixture of magnetite and maghaemite, the spectrum shifts from the magnetite sextet to the magnetite-plus-maghaemite sextet, and the area of the magnetite sextet decreases with increasing maghaemite. The proportion of maghaemite to ferrimagnetic minerals was calculated and checked against standard mixtures of magnetite and maghaemite according to the method of Solheid *et al.* (in preparation). Haematite, which has a hyperfine field of $B_{hf}=$ 51.8 T (fit no. 3 in Table 1), is also a major component of these extracts as well as of bulk samples, but it is not used in calculating relative maghaemite content.

Both bulk samples and magnetic extracts were analysed. Magnetic concentrates were made with a hand magnet. Measurements of σ_s before and after extraction showed that the process removed 50–75 per cent of the highly magnetic material from the bulk sample. While this procedure favours the larger magnetic grains, comparisons among the results are still useful.

The Mössbauer spectra for bulk samples are dominated by

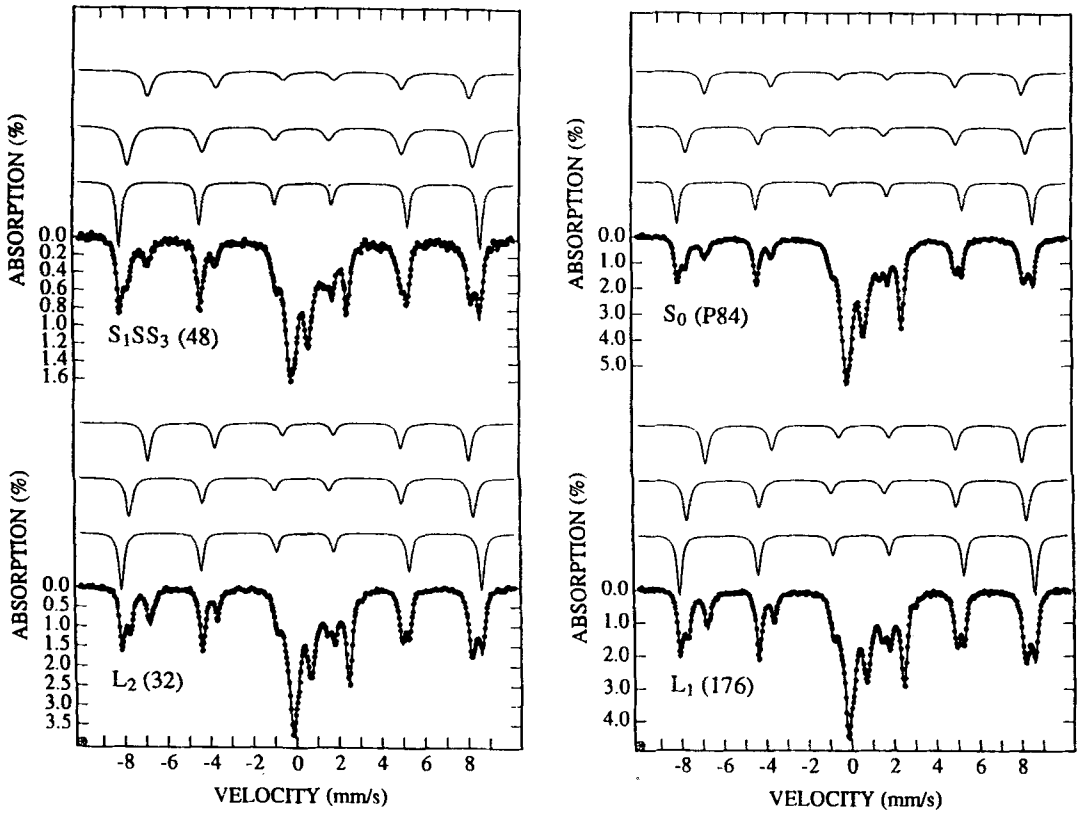

Figure 7. Mössbauer spectra for selected samples. Dots are the raw data, the top curve-fit is due to two-thirds of the magnetite, the middle curve-fit is due to one-third of the magnetite and all of the maghaemite, and the bottom curve-fit is due to haematite. The area below the baseline is proportional to the amount of material present.

Table 1. Results of Mössbauer analyses on magnetic extracts from two loesses and two palaeosols from the Xining site. The extracts consist of the coarser, more magnetic grains that could be removed with a hand magnet. The maghaemite/magnetite ratio is calculated using relative areas of curve-fits 1 and 2. Curve-fit 1 = two-thirds of the magnetite; curve-fit 2 = one-third of the magnetite plus all of the maghaemite; curve-fit 3 = all of the haematite.

Layer	Curve Fit	Hyperfine field B_{hf} (T)	Isomer Shift δ_{Fe} (mm s^{-1})	Quadrupole Splitting ΔE_Q (mm s^{-1})	Relative Area	γ-Fe_2O_3/(γ-Fe_2O_3+Fe_3O_4)
	1	46.3	0.660	–0.001	0.131	
S_0 (P84)	2	49.7	0.317	–0.059	0.161	0.33
	3	52.0	0.372	–0.182	0.173	
	remainder	—	—	—	0.546	
	1	46.3	0.668	–0.001	0.179	
L_1 (176)	2	49.7	0.302	–0.036	0.188	0.27
	3	52.0	0.371	–0.181	0.222	
	remainder	—	—	—	0.411	
	1	46.4	0.668	–0.024	0.141	
S_1 (48)	2	49.8	0.313	–0.083	0.230	0.43
	3	52.0	0.369	–0.170	0.210	
	remainder	—	—	—	0.419	
	1	46.3	0.669	–0.001	0.175	
L_2 (32)	2	49.7	0.306	–0.041	0.181	0.26
	3	52.0	0.370	–0.175	0.222	
	remainder	—	—	—	0.422	

the haematite sextet in both loess and palaeosol. In magnetic extracts, haematite, maghaemite, and magnetite are seen. Although haematite is the most abundant magnetic mineral, its magnetic signal is overwhelmed by the much stronger intrinsic magnetization of magnetite and maghaemite. Analysis of the spectra suggests that the maghaemite content of the ferrimagnetic fraction is approximately 26 per cent for L_2, 43 per cent for S_1, 27 per cent for L_1, and 33 per cent for S_0 (see Table 1). This analysis, which assumes that any maghaemite present is stoichiometric, yields maximum values for the maghaemite content.

Carbon

Measurements of total inorganic and organic carbon were carried out on approximately half of the samples as a non-magnetic means of evaluating the stratigraphy of the profile. Carbon measurements were completed using a Coulometrics automated carbon-dioxide coulometer. Total carbon was determined by combustion of approximately 100 mg of sediment at 950 °C to convert both organic and inorganic forms of carbon to CO_2. Total inorganic carbon was determined by the reaction of approximately 100 mg of fresh sediment with 2 ml of 2N $HClO_4$ solution to convert carbonate carbon to CO_2. The released CO_2 was passed through a titration cell, and the corresponding mass of carbon was determined. The difference between the total carbon and total inorganic carbon yielded the total organic carbon present in each sample with an uncertainty of 0.16 percentage points (Fig. 8).

Total organic carbon values are low throughout the profile, except within S_0 and S_1SS_3. Because organic carbon decomposes readily in an oxidizing loess environment, it is not well preserved except in the most strongly developed palaeosols.

Variations in inorganic carbon are more significant and can be used as a first approximation of the duration and intensity of pedogenic weathering during the period of formation of each of the individual units. Carbonate content has been used as an indicator of variations in monsoon-related precipitation on the Loess Plateau (Lu 1981; An *et al.* 1991, 1993; Liu & Ding 1993). Because measurements were not made to determine relative contributions of various forms of carbonate (for example calcite or dolomite), data are presented simply as percent inorganic carbon. In general, inorganic carbon is approximately 1.9 per cent (16 per cent $CaCO_3$ equivalent)

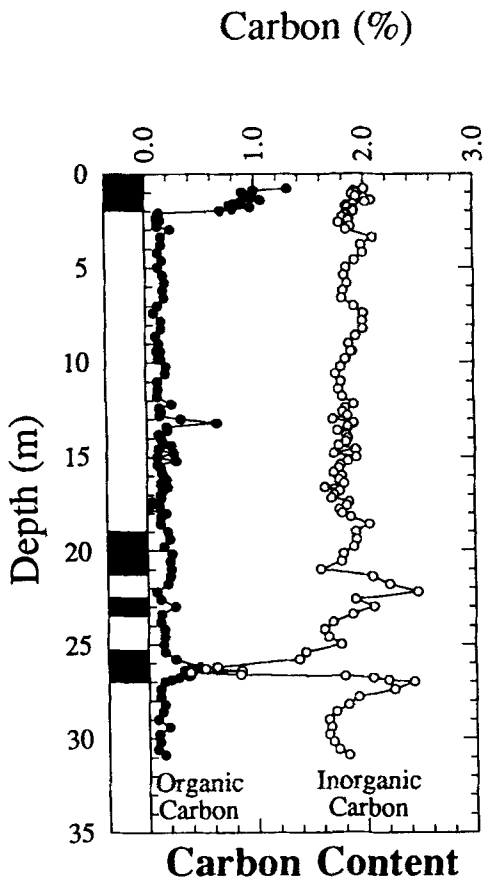

Figure 8. Weight percent of total organic carbon and total inorganic carbon for approximately half of the samples. Note the increased organic carbon in the two developed soils, S_0 and S_1SS_3, and the leaching and basal accumulation of inorganic carbon in S_1SS_1 and S_1SS_3. (To convert inorganic carbon to $CaCO_3$-equivalent, multiply by 8.333.)

throughout L_1 and varies in the range 0.4–2.5 per cent (3–20 per cent $CaCO_3$ equivalent) in the B and C horizons of S_1.

Comparisons between carbonate content and saturation magnetization variations (see Figs 2b and 8) demonstrate inverse correlations. Where magnetization values are highest, carbonate values are lowest. This is most pronounced within S_1SS_3, where peak interglacial weathering and soil formation occurred. Because saturation magnetization is a measure of the total concentration of magnetic minerals, this suggests that some decalcification and soil compaction occurred, especially in S_1SS_3.

DISCUSSION

To date, magnetic susceptibility has been the main magnetic proxy used for palaeoclimate reconstruction in the Chinese Loess Plateau. The mechanism through which the susceptibility record contains the global climate signal is important to climate models and to interpretation of magnetic data. Magnetic susceptibility enhancement in the palaeosol layers can be caused by variation in concentration, grain size, or mineralogy of the magnetic carrier. If the susceptibility signal had been purely the result of dilution of a uniform source material (as predicted by the magnetite-rain model), then the normalized susceptibility should be invariant with depth. Because it is not, there is some difference in magnetic mineralogy and/or grain size between the loess layers and the palaeosols.

Magnetic mineralogy

Magnetic mineralogy can be obtained from analysis of Mössbauer spectra, the temperature dependence of susceptibility, and low-temperature remanence transition data. Mössbauer results show that the ferrimagnetic composition of the magnetic extracts is approximately three-fifths to three-quarters magnetite and one-quarter to two-fifths maghaemite. There is also a considerable amount of haematite, which attaches itself to the more magnetic fraction (Table 1). This is similar to the conclusions of previous Mössbauer studies of loess and palaeosol (Han *et al.* 1991; Hus & Han 1992; Vandenberghe *et al.* 1992). The temperature dependence of susceptibility for bulk samples (Fig. 6) yields a common Curie point at approximately 575 °C, indicative of magnetite. For the two most mature soils (S_1SS_3 and S_0), the broad and sharp peaks in susceptibility are consistent with reduction of some maghaemite to magnetite because of CO_2 gas liberated from the organic fractions upon heating. Finally, the Verwey transition at approximately 118 K in the low-temperature remanence data (Fig. 4) also indicates the presence of magnetite in all samples.

Taken together, these results point to the presence of both magnetite and maghaemite in the loess/palaeosol complex. This is in contrast to those studies that claim to have found either only maghaemite (Eyre & Shaw 1994) or only magnetite (Evans & Heller 1994) in the most mature soils. In the latter case, because the reversibility of the temperature dependence of susceptibility curves is strongly dependent on the organic content of the samples, one cannot be sure without Mössbauer analysis that mature soil samples contain only magnetite.

Magnetic grain size

Magnetic granulometry can be achieved with analysis of the frequency dependence of susceptibility, hysteresis-loop parameters, and the thermal-demagnetization characteristics of a low-temperature saturation remanence. Such analyses on whole samples can only be qualitative—they give only the magnetic domain state or effective magnetic grain size. Yet, in the absence of a massive study of numerous separated magnetic grains in a transmission electron microscope, such qualitative conclusions are generally representative of the samples studied. For the purposes of this discussion, we will adopt the conventional grain-size assignments for magnetite: superparamagnetic (SP), $d < 30\,\text{nm}$; single-domain (SD), $30\,\text{nm} < d < 50\,\text{nm}$; pseudo-single-domain (PSD), $50\,\text{nm} < d < 8\,\mu\text{m}$; and multi-domain (MD), $d > 8\,\mu\text{m}$ (Dunlop 1973; Moskowitz & Banerjee 1979; Dunlop 1981).

The frequency dependence of susceptibility data (Fig. 5), obtained over a three decade frequency range, shows the presence of ample amounts of SP material in only the two most mature palaeosols, S_1SS_3 and S_0. Although this is in qualitative agreement with previous work, recent studies (Dearing *et al.* 1994; Forster, Evans & Heller 1994) suggest that the frequency dependence of susceptibility can rarely be interpreted quantitatively.

Another qualitative tool for grain-size study is the analysis of magnetic hysteresis-loop parameters. On a plot (not shown here) of the normalized saturation remanence (σ_{rs}/σ_s) against the coercivity ratio (H_{cr}/H_c) (after Day, Fuller & Schmidt 1977), the Xining hysteresis data fall in a range from the true MD to the middle of the PSD fields. However, this approach can lead to incorrect conclusions because of averaging of the extrema (Jackson, Worm & Banerjee 1990). It is thus not a sufficiently sensitive tool in this case where grain-size mixtures are certain to be present.

Instead of either of the above approaches, we rely on the relative variations of combinations of individual parameters such as ferrimagnetic susceptibility (χ_f), anhysteretic remanent magnetization (σ_{arm}), saturation isothermal remanent magnetization (σ_{rs}), and saturation magnetization (σ_s) (Figs 2 and 3). Variations with depth of saturation magnetization are the best estimates of concentration variations with depth of the strong magnetic fraction (magnetite and maghaemite). By normalizing the values of ferrimagnetic susceptibility with the corresponding values of saturation magnetization to obtain χ_f/σ_s (Fig. 2c), we can remove the effect of concentration variations with depth to see relative changes in the high-susceptibility grains of SP and MD sizes. Because MD grains are two-to-three times less susceptible than SP grains (Dunlop, Özdemir & Enkin 1987; Hunt, Moskowitz & Banerjee 1995), and because the absolute magnitude of the Verwey transition is approximately equal in all layers (suggesting a roughly uniform coarse-grained content), we can, as a first approximation, attribute all the variations in χ_f/σ_s to SP grains (Fig. 2c). We will discuss this in more detail in the next subsection.

The relative variations in the content of SD and PSD grains can be approximated by normalizing the anhysteretic remanence values with the corresponding saturation isothermal remanent magnetization values to obtain σ_{arm}/σ_{rs} (Fig. 3c). This ratio shows sharp increases in the palaeosols, confirming previous claims (Hus & Han 1992) that not only SP grains

but also SD and PSD grains are relatively enriched in these horizons. But, considering that the anhysteretic remanence acquired per unit field is approximately five times more effective than saturation remanence, and that normalized anhysteretic remanence values are only 1–2 per cent, the observed two-to-three-fold increase in σ_{arm}/σ_{rs} corresponds to only a small increase in the proportion of SD and PSD grains in the palaeosol layers.

The variations in saturation remanence represent changes in the absolute MD content, which is the bulk of the magnetic fraction. This parameter also show increases in the palaeosol layers. Similar variations in saturation remanence were also observed at Xifeng in the central Loess Plateau (Liu *et al.* 1992). Because the percentage variation of saturation remanence is greater than that of saturation magnetization, the former cannot be attributed to concentration variation alone. The only other possible variable is composition. Mössbauer data showed an increase in the proportion of maghaemite in the palaeosols. Because maghaemite has a higher coercivity, and by inference a higher saturation remanence, the remaining variations in saturation remanence could be attributed to variations in maghaemite content.

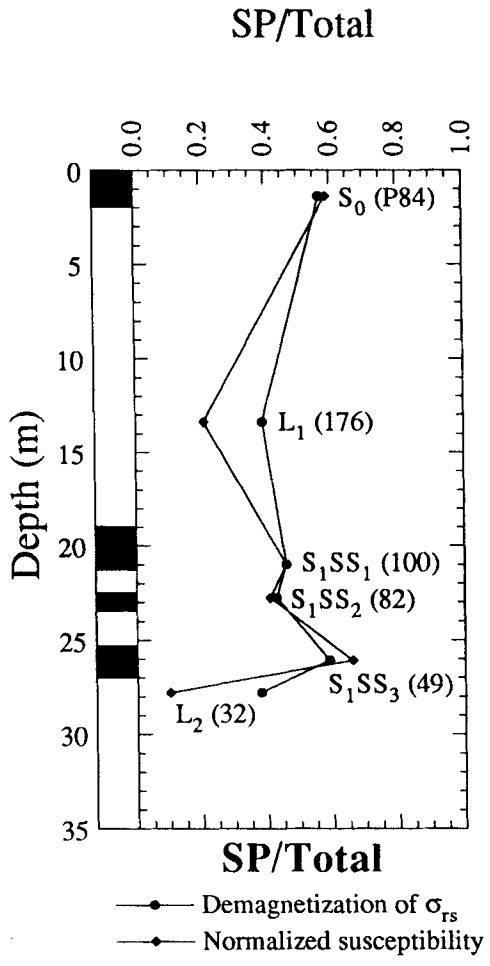

Figure 9. Estimates of SP content for selected samples by two methods: (1) proportion of low-temperature saturation magnetization that is carried by SP grains; (2) proportion of normalized susceptibility that is above the baseline signal (see text for details). The more developed palaeosols show the largest fraction, and the unweathered loesses show the least.

It appears, then, that palaeosols deposited during the warmer interglacials contain not only an excess of very small grains that dominate the χ_f/σ_s signal, but also the intermediate grains that carry σ_{arm} and the largest grains that carry σ_{rs}.

Superparamagnetic fraction

In the previous section, we suggested that normalized ferrimagnetic susceptibility (χ_f/σ_s), rather than raw susceptibility (χ), represents best the concentration-independent variations in the SP fraction. In the absence of a baseline value of χ_f/σ_s corresponding to pristine unaltered loess with an SP fraction presumably near zero, we chose the baseline to be the lowest measured value (5.7×10^{-6} m A^{-1}, obtained from sample 33 in the L_2 layer at 27.7 m depth). When increases in χ_f/σ_s (assumed for our purposes to be due to SP material) are measured with reference to this baseline, SP fractions lie in the range from approximately 25 per cent in most other loess samples to a maximum of 66 per cent in S_1SS_3 (Fig. 9). This approach exaggerates the contrasts by neglecting the other contributions to the susceptibility (MD, and to a lesser extent PSD and SD), and by not using an unaltered loess for the background value.

The values for SP content obtained using χ_f/σ_s nevertheless compare favourably with the more reliable thermal demagnetization of low-temperature saturation remanence technique. The difference between the two methods is large only for the glacial layers L_1 and L_2. For the interglacial layers, S_0, S_1SS_1, S_1SS_2, and S_1 SS_3, the two methods give comparable results (Fig. 9). Although Xining is now situated in a relatively arid part of the Loess Plateau, during the early Holocene and during marine oxygen isotope stage 5e, SP fractions were as high as 57 and 59 per cent respectively. Although the interpretation of normalized susceptibility is not as clear as the low-temperature method, the normalized susceptibility technique nevertheless gives reasonable results, is easier to perform, and represents an important rock-magnetic improvement over using susceptibility alone.

SP fractions and pedogenesis

Earlier workers have correlated SP fractions, as measured by differences in raw susceptibility, with intensity of pedogenesis. While this approach is probably justified at least approximately, we contend that an improvement on this technique is either to normalize for concentration variation of the magnetic species (χ_f/σ_s) or to use thermal demagnetization of low-temperature saturation remanence to measure SP fractions more accurately. If we then make the assumption that all SP grains are produced by pedogenesis, we can treat the data of Fig. 9 as representing relative variations in pedogenesis.

Fig. 10 shows a comparison of raw susceptibility profiles from Xining compared with previously published data from three other nearby sites in the western Loess Plateau: Beiyuan (An *et al.* 1991), Jiuzhoutai/Lanzhou (Chen, Li & Zhang 1991) and Baicaoyuan (Evans & Heller 1994). The overall agreement among the four sites is self-evident. Yet, the perils of directly attributing the variation in susceptibility to intensities of relative pedogenesis can also be seen in Fig. 10. Raw susceptibility data from Beiyuan and Lanzhou appear to suggest that the climates during the early Holocene and stage 5e were similarly warm and humid, while the data from Baicaoyuan

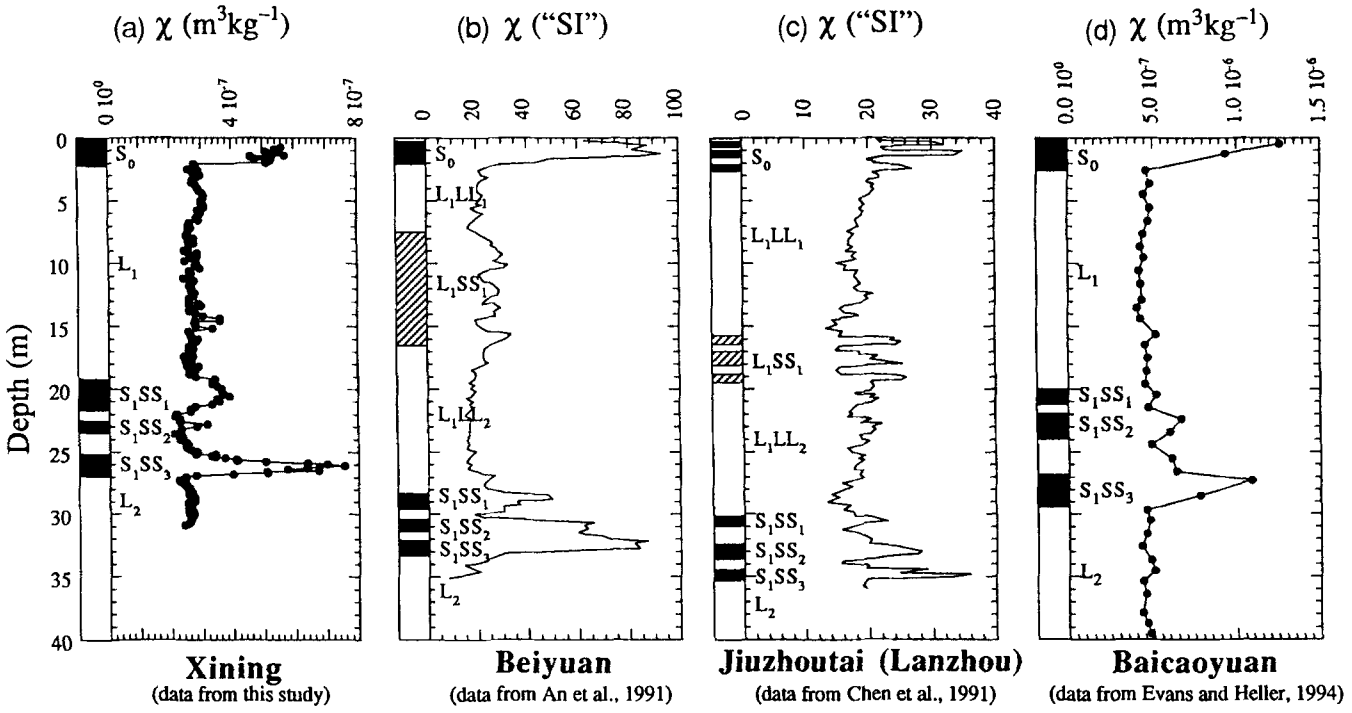

Figure 10. Susceptibility profiles for other sites in the Loess Plateau. Western sites: (a) Xining (36.6°N, 101.7°E); (b) Beiyuan (35.6°N, 103.2°E); (c) Lanzhou/Jiuzhoutai (36.1°N, 103.8°E); and (d) Baicaoyuan (36.2°N, 105.0°E). Note the relatively subdued L_1SS_1 layer and the relatively well-articulated sublayers in S_1.

suggest that the Holocene was warmer and more humid, and the data from Xining suggest the opposite. This rather paradoxical situation can be resolved by removing the concentration dependence of the magnetic species through normalization to obtain a more reliable estimate of the SP fraction and presumably of the intensity of pedogenesis. Reference to Figs 2(c) and 9 shows that the stage-5e palaeosol development was indeed more intense, and therefore that the climate was probably warmer and more humid during stage 5e than during the early Holocene in the western Loess Plateau. This conclusion is compatible with globally averaged $\delta^{18}O$ data.

Despite the problems encountered when using susceptibility alone as a measure of pedogenesis, it is still clear from Fig. 10 that the climate during marine oxygen isotope stage 3 resulted in very little pedogenesis in the western sites. This is in contrast with stronger palaeosol development during the same time interval, as noted at Xifeng (Fig. 11) and Luochuan (Kukla 1987) in the east. At Baicaoyuan and Xining, the stage-3 soil (L_1SS_1) appears to be non-existent, while in the other two western sites it is only very poorly developed. This conclusion becomes more rigorous when concentration-independent SP fractions (as measured by χ_f/σ_s) are compared for eastern and western sites (Fig. 11).

CONCLUSIONS

Correct normalization of magnetic parameters is both useful and necessary in order to reduce the number of variables in magnetic climate proxy studies. In the Loess Plateau, the fine-grained magnetic signal, often assumed to be a pedogenic signal, is measured more accurately by the ferrimagnetic susceptibility normalized by saturation magnetization, χ_f/σ_s, and by the anhysteretic remanence normalized by the saturation remanence, σ_{arm}/σ_{rs}. Use of normalized parameters gives results comparable to more rigorous methods such as thermal demagnetization of low-temperature saturation remanence. Because the techniques used here are still new, caution should be exercised until further work has been done.

A comparison among the better-known western sites (Xining, Beiyuan, Lanzhou and Baicaoyuan) yields comparable magnetic climate proxy characteristics which provide an average picture of the climate in the western Loess Plateau. Because pedogenesis was not as intense in the west, the stage-3 immature soil within the Malan loess, L_1SS_1, is difficult to find. On the other hand, the three substages in S_1 (corresponding to marine isotope substages 5a, 5c, and 5e) have precise and sharp boundaries.

These local characteristics contrast with those of a typical eastern site (Xifeng), in which L_1SS_1 is magnetically well defined, but variations in the magnetic signal during the three substages of S_1 are seen to be due mostly to concentration variation. We hope that in the future, detailed magnetic and non-magnetic data will become available throughout the Loess Plateau, so that further comparisons among sites can be made.

ACKNOWLEDGMENTS

We thank Dr Li Zhen of the Department of Geology, Qinghai Normal University, Xining, for invaluable assistance in the field, and two anonymous reviewers for useful comments and suggestions which improved the manuscript. This research was funded by the US National Science Foundation (grant EAR/9206024 with travel supplement) and the Chinese National Natural Science Foundation (grant 49272426). Dr Han's stay at the Institute for Rock Magnetism was supported in part by the University of Minnesota Graduate School, and

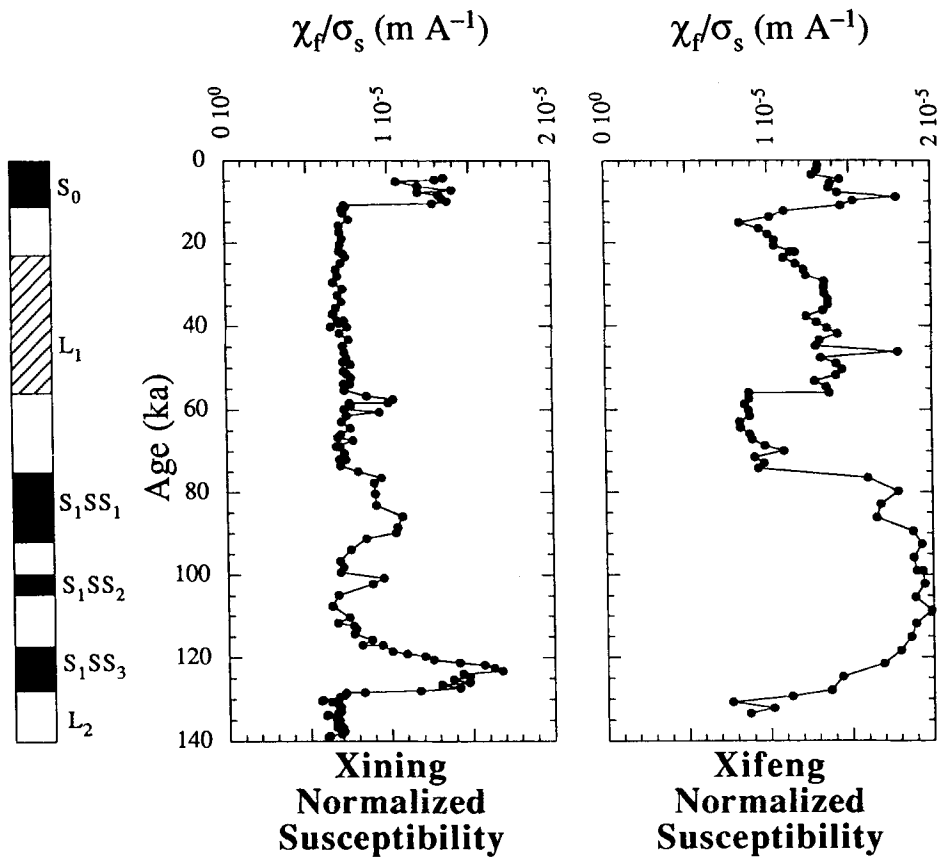

Figure 11. Comparison of normalized susceptibility profiles from Xining (36.6°N, 101.7°E) in the western Loess Plateau and Xifeng (35.7°N, 107.7°E) in the eastern Loess Plateau.

his international travel expenses were provided by the Chinese National Natural Science Foundation. This paper is contribution number 9411 of the Institute for Rock Magnetism, which functions with the support of the W.M. Keck Foundation, the US National Science Foundation, and the University of Minnesota.

REFERENCES

An, Z.-S., Kukla, G.J., Porter, S.C. & Xiao, J., 1991. Magnetic susceptibility evidence of monsoon variation on the loess plateau of central China during the last 130,000 years, *Q. Res.*, **36**, 29–36.

An, Z.-S. *et al.*, 1993. Episode of strengthened summer monsoon climate of Younger Dryas age on the loess plateau of central China, *Q. Res.*, **39**, 45–54.

Baksi, A.K., Hsu, V., McWilliams, M.O. & Farrar, E., 1992. $^{40}Ar/^{39}Ar$ dating of the Brunhés–Matuyama geomagnetic field reversal, *Science*, **256**, 356–357.

Banerjee, S.K., 1995. Chasing the paleomonsoon over China: its magnetic proxy record, *GSA Today*, **5**, 93–97.

Banerjee, S.K., Hunt, C.P. & Liu, X.-M., 1993. Separation of local signals from the regional paleomonsoon record of the Chinese loess plateau: a rock-magnetic approach, *Geophys. Res. Lett.*, **20**, 843–846.

Bassinot, F.C., Labeyrie, L.D., Vincent, E., Quidelleur, X., Shackleton, N.J. & Lancelot, Y., 1994. The astronomical theory of climate and the age of the Brunhés–Matuyama magnetic reversal, *Earth planet. Sci. Lett.*, **126**, 91–108.

Bean, C.P. & Livingston, J.D., 1959. Superparamagnetism, *J. appl. Phys.*, **30**, 120S–129S.

Bloemendal, J., Barton, C.E. & Radhakrishnamurty, C., 1985. Correlation between Rayleigh loops and frequency-dependent and quadrature susceptibility: application to magnetic granulometry of rocks, *J. Geophys. Res. B*, **90**, 8789–8792.

Chen, F.-H., Li, J.-J. & Zhang, W.-X., 1991. Loess stratigraphy of the Lanzhou profile and its comparison with deep-sea sediment and ice core record, *GeoJournal*, **24**, 201–209.

Cullity, B.D., 1972. *Introduction to Magnetic Materials*, Addison-Wesley, Reading, MA.

Day, R., Fuller, M. & Schmidt, V.A., 1977. Hysteresis properties of titanomagnetites: grain-size and compositional dependence, *Phys. Earth planet. Inter.*, **13**, 260–266.

Dearing, J.A., Dann, R., Lees, J.A. & Maher, B.A., 1994. Frequency dependent susceptibility measurements of soils (abstract), *Ann. Geophys.*, **12**(suppl. 1), C163.

Dunlop, D.J., 1973. Superparamagnetic and single-domain threshold sizes in magnetite, *J. Geophys. Res.*, **78**, 1780–1793.

Dunlop, D.J., 1981. The rock magnetism of fine particles, *Phys. Earth planet. Inter.* **26**, 1–26.

Dunlop, D.J., Özdemir, Ö. & Enkin, R.J., 1987. Multidomain and single-domain relations between susceptibility and coercive force, *Phys. Earth planet. Inter.*, **49**, 181–191.

Evans, M.E. & Heller, F., 1994. Magnetic enhancement and palaeoclimate: study of a loess/palaeosol couplet across the loess plateau of China, *Geophys. J. Int.*, **117**, 257–264.

Eyre, J.K. & Shaw, J., 1994. Magnetic enhancement of Chinese loess—the role of γ-Fe_2O_3?, *Geophys. J. Int.*, **117**, 265–271.

Forster, T., Evans, M.E. & Heller, F., 1994. The frequency dependence of low field susceptibility in loess sediments, *Geophys. J. Int.*, **118**, 636–642.

Han, J.-M., Hus, J.J., Paepe, R., Vandenberghe, R.E. & Liu, T.-S., 1991. The rock magnetic properties of the Malan and Lishi forma-

tions in the loess plateau of China, in *Loess, Environment, and Global Change*, pp. 30–47, ed. Liu, T.-S., Science Press, Beijing.

Heller, F. & Liu, T.-S., 1984. Magnetism of Chinese loess deposits, *Geophys. J. R. astr. Soc.*, **77**, 125–141.

Heller, F. & Liu, T.-S., 1986. Palaeoclimatic and sedimentary history from magnetic susceptibility of loess in China, *Geophys. Res. Lett.*, **13**, 1169–1172.

Heller, F., Shen, C.-D., Beer, J., Liu, X.-M., Liu, T.-S., Bronger, A., Suter, M. & Bonani, G., 1993. Quantitative estimates of pedogenic ferromagnetic mineral formation in Chinese loess and palaeoclimatic implications, *Earth planet. Sci. Lett.*, **114**, 385–390.

Hovan, S.A., Rea, D.K., Pisias, N.G. & Shackleton, N.J., 1989. A direct link between the China loess and marine $\delta^{18}O$ records: aeolian flux to the north Pacific, *Nature*, **340**, 296–298.

Hunt, C.P. & Banerjee, S.K., 1992. Thermal demagnetization of low-temperature SIRM: a new method for magnetic granulometry (abstract), *EOS, Trans. Am. geophys. Un.* **73**(43 suppl.), 138.

Hunt, C.P., Moskowitz, B.M. & Banerjee, S.K., 1995. Magnetic properties of rocks and minerals, in *Handbook of Physical Constants*, ed. Ahrens, T.J., Am. Geophys. Un., Washington, DC, **3**, 189–204.

Hus, J.J. & Han, J.-M., 1992. The contribution of loess magnetism in China to the retrieval of past global changes—some problems, *Phys. Earth planet. Inter.*, **70**, 154–168.

Imbrie, J. *et al.*, 1984. The orbital theory of Pleistocene climate: support from a revised chronology of the marine $\delta^{18}O$ record, in *Milankovitch and Climate: Understanding the Response to Orbital Forcing*, pp. 269–305, eds Berger, A., Imbrie, J., Hays, J., Kukla, G. & Saltzman, B., Reidel Publishing, Dordrecht.

Jackson, M.J., Worm, H.-U. & Banerjee, S.K., 1990. Fourier analysis of digital hysteresis data: rock magnetic applications, *Phys. Earth planet. Inter.*, **65**, 78–87.

Kukla, G.J., 1987. Loess stratigraphy in central China, *Q. Sci. Rev.*, **6**, 191–219.

Kukla, G.J. & An, Z.-S., 1989. Loess stratigraphy in central China, *Palaeogeog. Palaeoclimat. Palaeoecol.*, **72**, 203–225.

Kukla, G.J., Heller, F., Liu, X.-M., Xu, T.-C., Liu, T.-S. & An, Z.-S., 1988. Pleistocene climates dated by magnetic susceptibility. *Geology*, **16**, 811–814.

Li, Z., Ma, H.-Z. & Zeng, Y.-N., 1992. A preliminary study on the Dadunling loess profile of Xining. *Geol. Qinghai*, **1**, 26–32 (in Chinese).

Liu, T.-S., ed., 1991. *Loess, Environment, and Global Change*, Science Press, Beijing.

Liu, T.-S. & Ding, Z.-L., 1993. Stepwise coupling of monsoon circulations to global ice volume variations during the Late Cenozoic, *Global Planet. Change*, **7**, 119–130.

Liu, X.-M., Shaw, J., Liu, T.-S., Heller, F. & Baoyin, Y., 1992. Magnetic mineralogy of Chinese loess and its significance, *Geophys. J. Int.*, **108**, 301–308.

Liu, X.-M., Bloemendal, J., Rolph, T., Shaw, J., Liu, T.-S. & Heller, F., 1995. Quantitative estimates of palaeoprecipitation in the loess plateau of China. *Palaeogeog. Palaeoclimat. Palaeoecol*, in press.

Lu, Y.-C., 1981. Pleistocene climatic cycles and variations of $CaCO_3$ contents in a loess profile, *Sci. Geol. Sin.*, **2**, 122–131 (in Chinese).

Maher, B.A. & Taylor, R.M., 1988. Formation of ultrafine-grained magnetite in soils, *Nature*, **336**, 368–371.

Maher, B.A. & Thompson, R., 1991. Mineral magnetic record of the Chinese loess and paleosols, *Geology*, **19**, 3–6.

Maher, B.A. & Thompson, R., 1992. Paleoclimatic significance of the mineral magnetic record of the Chinese loess and paleosols, *Q. Res.*, **37**, 155–170.

Maher, B.A., Thompson, R. & Zhou, L.-P., 1994. Spatial and temporal reconstructions of changes in the Asian palaeomonsoon: a new mineral magnetic approach, *Earth planet. Sci. Lett.*, **125**, 462–471.

Moskowitz, B.M. & Banerjee, S.K., 1979. Grain size limits for pseudo-single-domain behavior in magnetite: implications for paleomagnetism, *IEEE Trans. Magn.*, **MAG-15**, 1241–1246.

Néel, L., 1949. Influence des fluctuations thermiques sur l'aimantation de grains ferromagnétiques trés fins, *C. R. Acad. Sci. (Paris), Sér. B*, **228**, 664–666.

Oldfield, F., Chen, F.-H. & Wu, R.-J., 1994. Magnetic property and particle size variations in the Late Pleistocene and Holocene parts of the Dadongling loess section near Xining, China (abstract), *INQUA/QRA Abstr. Papers Posters*, **14**.

Özdemir, Ö., Dunlop, D.J. & Moskowitz, B.M., 1993. The effect of oxidation of the Verwey transition in magnetite, *Geophys. Res. Lett.*, **20**, 1671–1674.

Radhakrishnamurty, C. & Deutsch, E.R., 1974. Magnetic techniques for ascertaining the nature of iron oxide grains in basalts, *J. Geophys.*, **40**, 453–465.

Solheid, P.A., Banerjee, S.K. & Moskowitz, B.M., 1995. Mössbauer spectroscopy as a means of determining relative magnetic mineralogy in loess-paleosol sequences of China, in preparation.

Stephenson, A., 1971. Single domain grain distributions I. A method for the determination of single domain grain distributions, *Phys. Earth planet. Inter.*, **4**, 353–360.

Vandenberghe, R.E., De Grave, E., Landuydt, C. & Bowen, L.H., 1990. Some aspects concerning the characterization of iron oxides and hydroxides in soils and clays, *Hyperfine Interact.*, **53**, 175–195.

Vandenberghe, R.E., De Grave, E., Hus, J.J. & Han, J.-M., 1992. Characterization of Chinese loess and associated palaeosol by Mössbauer spectroscopy, *Hyperfine Interact.*, **70**, 977–980.

Verosub, K.L., Fine, P., Singer, M.J. & TenPas, J., 1993. Pedogenesis and paleoclimate: interpretation of the magnetic susceptibility record of Chinese loess–paleosol sequences, *Geology*, **21**, 1011–1014.

Zhou, L.-P., Oldfield, F., Wintle, A.G., Robinson, S.G. & Wang, J.T., 1990. Partly pedogenic origin of magnetic variations in Chinese loess, *Nature*, **346**, 737–739.